*Journal of Marine Research, 52,* 837–863, 1994

# Instability waves in the Gulf Stream front and its thermocline layer

**by Sang-Ki Lee[1] and G. T. Csanady[1]**

ABSTRACT

We carried out linear instability calculations on a three layer Gulf Stream front model in an attempt to elucidate the interaction of the thermocline layer with surface slopewater shoreward of the front. The basic state is geostrophic balance and constant potential vorticity in the two active layers, but the perturbations are ageostrophic. We found the flow to be unstable to long wave perturbations, the wavelength of the most unstable wave to be of the order of 10 radii of deformation. The instability is mainly baroclinic, 75–85% of the energy supply to the growing perturbation coming from basic flow potential energy. Calculated wavelengths, phase speeds and growth rates, using parameters typical of the Gulf Stream, are similar to those observed. The eigenfunctions of the perturbations show peak cross-front thermocline motions near the inflection points of a frontal wave, and a cyclonic eddy with closed streamlines under a trough, an anticyclonic eddy under a crest. The combined flow (basic state plus perturbation) in the thermocline layer follows the surface streamlines closely, except for small cross-stream anomalies, shoreward just upstream of a wave crest, seaward upstream of a trough. Calculated trajectories have characteristics similar to those observed by RAFOS floats, except that they suggest exchange of thermocline waters exclusively with slopewater.

## 1. Introduction

### *a. Slope Sea and Gulf Stream thermocline*

Upon separation from the coast, western boundary currents develop unstable waves of spectacular amplitude, affecting a large neighboring region. The instability of the Gulf Stream, in particular, is responsible for great variability of currents and water properties north of Cape Hatteras, in the Slope Sea, the 100 km or so wide strip of the ocean between the Stream and the continental slope. Where not occupied by Gulf Stream meanders or rings, the surface layers of the Slope Sea contain the distinctive water mass known as slopewater (Iselin, 1936). As Rossby (1936) recognized, this water mass is in contact along isopycnal surfaces with thermocline waters under the Gulf Stream, and differs from them only by a slight salinity deficit (McLellan *et al.,* 1953). Csanady and Hamilton (1988) pointed out that the seasonal cycle of pycnostad formation and erosion in the surface layers of the

1. Center for Coastal Physical Oceanography, Old Dominion University, Norfolk, Virginia 23529-0276, U.S.A.

Slope Sea requires constant replenishment of thermocline waters from under the Gulf Stream. Because there is no significant net shoreward advection along the isopycnal surfaces in question (Bower *et al.,* 1985), the replenishment must be effected by eddy mixing. It is reasonable to suppose that unstable wave motions, developing into eddies at finite amplitude are responsible for this.

Another aspect of Gulf Stream influence on the Slope Sea was brought to light by Bane *et al.* (1988), who reported that when a Gulf Stream meander approaches the continental margin, displacing surface slopewater, the southward flow of the upper slope current of the Mid-Atlantic Bight speeds up. Csanady and Hamilton (1988) suggested that the upper slope current is one leg of a closed western Slope Sea gyre. If this is true, squeezing the gyre by a Gulf Stream meander apparently speeds it up. The approach to the coast of a meander of course means that the surface layer of the Gulf Stream moves shoreward. Thermocline waters, which are in contact with the surface waters of the Slope Sea, may conceivably move seaward at the same time, creating a void which the upper slope current has to fill. Whatever the exact explanation, there is clearly a connection between the movements of Gulf Stream thermocline waters and Slope Sea waters, associated with the unstable waves of the boundary current. The motivation for our study was the desire to understand movements of thermocline waters under and around a separated western boundary current.

*b. Modeling requirements*

In order to portray motions in the thermocline of a separated boundary current by a simple model, a minimum of two active layers are necessary: one, the surface layer, terminating in a surface outcrop, two, a layer under the surface layer seaward of the outcrop, becoming the surface layer shoreward. Underlying both, in the simplest approach, there is a deep inert layer. In the belief that meander and eddy motions observed in a separated boundary current are finite amplitude developments of instability waves, we analyze the stability of a basic state containing an upwelled front and a baroclinic current. As is standard in such analysis, we suppose a frictionless fluid, and small perturbations leading to linearized equations of motion. It is reasonable to suppose that this approach correctly quantifies such key properties of Gulf Stream meanders as phase speed, growth rate, and wavelength of the dominant wave, provided that the basic state is physically realizable and representative of the separated boundary current. The structure (eigenfunctions) of the instability waves should also give clues to the character and range of eddy motions developing as the amplitude of the disturbances becomes large. Detailed agreement with observed finite amplitude motions should not, however, be expected of small perturbation theory.

The requirement of a realistic and representative basic state excludes the quasigeostrophic approach, as Garvine (1984) and Killworth *et al.* (1984) have pointed out: in

the separated Gulf Stream the Rossby number is of order one. Both these papers treat a single active layer model of the Gulf Stream, with Stommel's (1965) constant potential vorticity surface layer as the basic state (Killworth *et al.* explored other basic states, too). Constant potential vorticity in two or three active layers yields models of finite amplitude coastal upwelling (Csanady, 1982), and is also a suitable basic state for instability wave analysis on a separated boundary current with an active thermocline layer. We used a two active layer version of this model, with the third, bottom, layer at rest in the basic state, but containing perturbation motions. Boundary conditions were evanescent motion at infinity on both sides of the outcrop, or a coastal wall limiting the surfaced thermocline layer, where the normal velocity vanishes.

*c. Earlier studies of frontal instability waves*

Theoretical studies of oceanic frontal instability originate from Orlanski's (1968) pioneering paper, in which he examined the instability of the (atmospheric) Norwegian polar front. The basic state was a plane inclined interface intersecting rigid top and bottom boundaries, and separating two fluids of different density. Model results showed that the front was unstable at all wavelengths. Rayleigh shear instability, Kelvin-Helmholtz instability and baroclinic instability were all found to operate in some portion of wavenumber space.

Following Orlanski's work, a number of stability studies have been carried out on atmospheric and oceanic fronts using quasi-geostrophic theory (a basic state with small Rossby number). The trend of recent work has been away from QG theory, notable examples being the studies of Paldor (1983), Killworth (1983) and Killworth *et al.* (1984), all using the shallow water equations.

Paldor (1983) studied the instability of an "isolated" (upwelled) surface front using a simple reduced gravity model (1½ layer model). The basic state in the model had an active top layer of constant potential vorticity, and an infinitely deep bottom layer. He found this state to be unconditionally stable, but supporting trapped waves of zero growth rate moving either downstream or upstream. Killworth (1983) examined a slightly extended model. He allowed non-uniform potential vorticity in the basic state, and showed that the flow was unstable if the basic potential vorticity decreased toward the front. Interestingly, the criterion for instability found by Killworth (1983) is clearly different from what QG theory suggests, which is that the basic potential vorticity must change sign somewhere inside the fluid (Pedlosky, 1987). Or in a two-layer QG model, the basic potential vorticity gradients in the two layers must have different signs (Phillips, 1954; Pedlosky, 1962; Orlanski, 1969).

The 1½ layer models include stratification in a highly simplified form, but eliminating perturbations in a second layer prevents baroclinic instability. The models of Killworth (1983), Garvine (1984) and Kubokawa (1985) all suffer from this constraint. Laboratory experiments (Chia *et al.,* 1982; Griffiths and Linden, 1982),

which all have active bottom layers, reveal frontal instability growth rates much larger than found by Killworth (1983). In order to account for this, Killworth *et al.* (1984) developed a two-layer model, allowing perturbations in the bottom layer, although in the basic state only the top layer was in motion, the bottom layer stagnant (a similar model was previously studied by Orlanski (1969)). Killworth *et al.* (1984) obtained unstable waves regardless of the distribution of the basic potential vorticity. This model reproduced the growth rate of the most unstable wave in the laboratory experiments of Chia *et al.* (1982) and Griffiths and Linden (1982).

Two-layer models, laboratory or analytical, cannot in principle portray thermocline motions in a separated boundary current. Therefore we use a simplified three-layer model of a separated boundary current, in an attempt to understand the effect of an active thermocline layer on the stability of the flow and especially to reveal details of instability wave motions in the thermocline layer.

We also analyze energy exchange between the geostrophic basic flow and the perturbations.

## 2. Formulation of the problem

### *a. The model*

The model configuration, Figure 1, shows two fluids of uniform densities $\rho_1$ and $\rho_2$, flowing above a fluid of density $\rho_3$ where $\rho_1 < \rho_2 < \rho_3$. The basic flow is taken to be geostrophic in the upper two layers, parallel to the $x$-axis, and stagnant in the bottom layer. The interface between the upper two layers intersects the surface at $y = 0$ and their depths approach constant values, $H_1$ and $H_2$, as $y \to \pm\infty$ for an "isolated" front. A "coastal" front terminates motion at $y = y_c$ where the depth is $h_2(y_c) \geq H_2$. The model domain is divided into two zones: to the right of the front (from $y = 0$ to $y = \infty$ for the isolated front, from $y = 0$ to $y = y_c$ for the coastal front) is a two-layer fluid defined as *Zone I* and to the left (from $y = -\infty$ to $y = 0$) is a three-layer fluid defined as *Zone II*. Let $\gamma$ be the ratio of the total depth ($H_T$) to the top layer thickness ($H_1$) and $\delta$ be the ratio of the thermocline layer thickness ($H_2$) to that of the top layer ($H_1$) at $y = -\infty$ so that, after some minor manipulations, the bottom layer thickness becomes $H_1(\gamma - 1 - \delta)$ at $y = -\infty$, and $H_1(\gamma - \delta)$ at $y = \infty$ for the isolated front, $h_3 \leq H_1(\gamma - \delta)$ at $y = y_c$ for the coastal front.

The variables are made nondimensional as follows:

$$
\begin{aligned}
t^* &= tf^{-1} \\
x^* &= x\sqrt{g\epsilon_{21}H_1}f^{-1}, \qquad & y^* &= y\sqrt{g\epsilon_{21}H_1}f^{-1}, \\
u^* &= u\sqrt{g\epsilon_{21}H_1}, & v^* &= v\sqrt{g\epsilon_{21}H_1}, \\
\eta_1^* &= \eta_1\epsilon_{21}H_1, & h_1^* &= h_1H_1, \\
\eta_2^* &= \eta_2\epsilon_{21}H_1, & h_2^* &= h_2H_2,
\end{aligned}
\tag{1}
$$

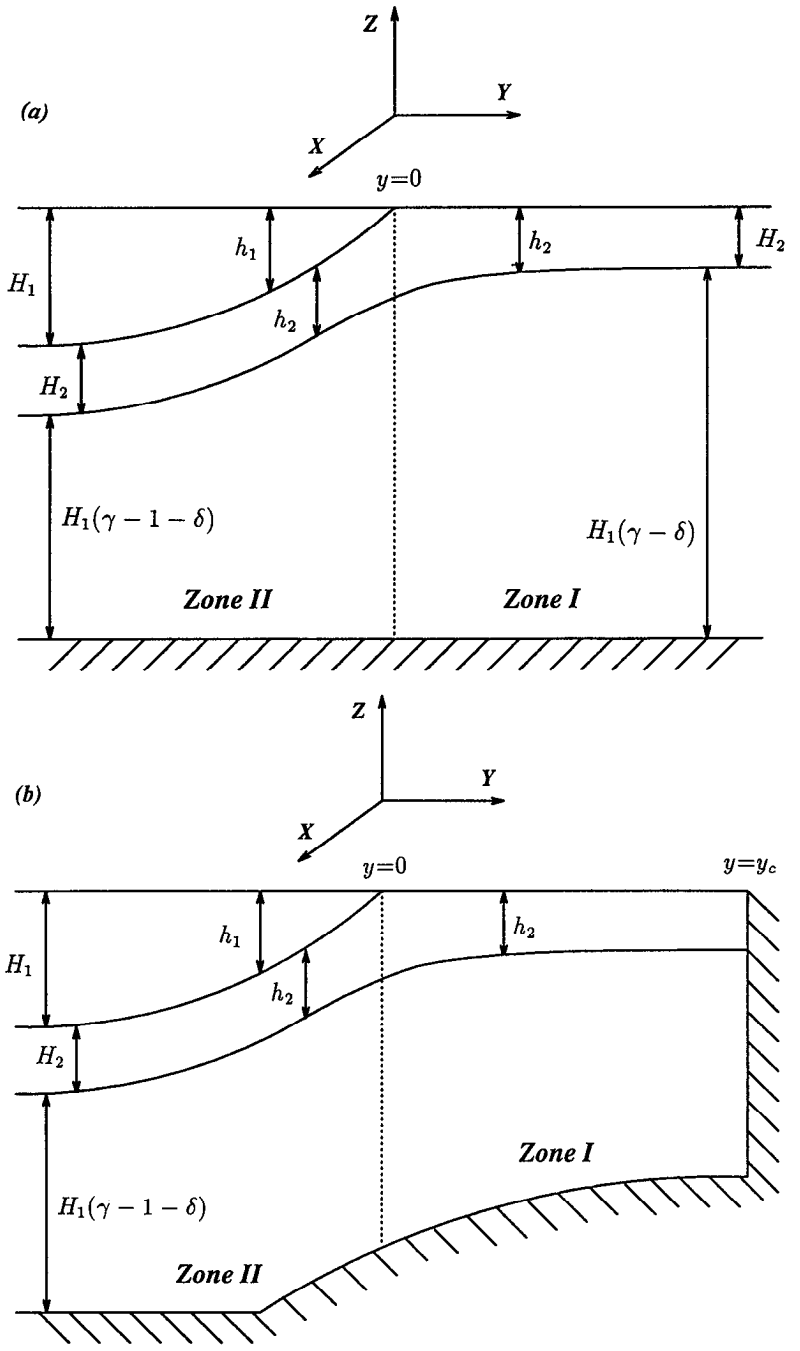


Figure 1. The configuration for the three-layer model: (a) isolated front, (b) coastal front.

where $f$ is the Coriolis parameter, $g$ is acceleration of gravity, $h_1^*$ and $h_2^*$ are the dimensional layer thicknesses of top and thermocline layers, $\eta_1^*$ and $\eta_2^*$ are the free surface elevations for *Zone II* and *Zone I* respectively, $\sqrt{g\epsilon_{21}H_1}f^{-1}$ is the internal deformation radius, and $\epsilon_{21}$ is given by

$$\epsilon_{21} = 1 - \frac{\rho_1}{\rho_2}.$$

*b. The basic state*

In the basic state we prescribe geostrophic balance and constant potential vorticity, for both active layers (Csanady, 1982; Huang and Stommel, 1990). Nondimensional equations describing this state are:

$$\left.\begin{aligned} \bar{u}_1 &= -(\alpha + 1)\bar{h}_{1y} - \alpha\delta\bar{h}_{2y} \\ \bar{h}_1 &= 1 - \bar{u}_{1y} \end{aligned}\right\} \qquad y < 0, \tag{2}$$

$$\bar{u}_2 = -\alpha\bar{h}_{1y} - \alpha\delta\bar{h}_{2y} \tag{3}$$

$$\bar{h}_2 = 1 - \bar{u}_{2y} \tag{4}$$

$$\bar{u}_1 = \bar{h}_1 = 0 \qquad y > 0, \tag{5}$$

where $\delta$ is defined in Section 2a and

$$\alpha = \frac{\rho_3 - \rho_2}{\rho_2 - \rho_1} \tag{6}$$

is a stratification ratio.

The solution satisfying the boundary conditions at infinity ($\bar{u}_y = 0$ at $y \to \pm\infty$) is:

$$\left.\begin{aligned} \bar{h}_1 &= a_1 e^{r_1 y} + a_2 e^{r_2 y} + 1 \\ \bar{h}_2 &= b_1 e^{r_1 y} + b_2 e^{r_2 y} + 1 \end{aligned}\right\} y \le 0, \tag{7}$$

$$\left.\begin{aligned} \bar{h}_1 &= 0 \\ \bar{h}_2 &= c_3 e^{-r_3 y} + 1 \end{aligned}\right\} \qquad y \ge 0, \tag{8}$$

where

$$r_{1,2} = \sqrt{\frac{(\alpha + 1 + \alpha\delta) \pm \sqrt{(\alpha + 1 + \alpha\delta)^2 - 4\alpha}}{2\alpha\delta}}, \tag{9}$$

$$r_3 = -\sqrt{1/\alpha\delta}, \tag{10}$$

$$b_i = \frac{1 - \alpha\delta r_i^2}{\alpha r_i^2} a_i, \qquad i = 1, 2. \tag{11}$$

The constants $a_1$, $a_2$ and $c_3$ follow from matching conditions at $y = 0$: $\bar{h}_1 = 0$, $\bar{h}_2$ and $\bar{u}_2$ continuous:

$$\left.\begin{aligned} 1 + a_1 + a_2 &= 0, \\ 1 + b_1 + b_2 &= 1 + c_3, \\ r_1 a_1 + r_2 a_2 + \delta r_1 b_1 + \delta r_2 b_2 &= -\delta r_3 c_3. \end{aligned}\right\} \tag{12}$$

For $\alpha = 1$ and $\delta = 1$, the constants are:

| | | | |
|---|---|---|---|
| $a_1$ | −0.381966 | $a_2$ | −0.618034 |
| $b_1$ | +0.618034 | $b_2$ | −0.381966 |
| $c_3$ | +0.236068 | $r_3$ | +1.000000 |
| $r_1$ | +1.618030 | $r_2$ | +0.618034 |

The basic state for the coastal front is obtained with vanishing velocity at the coast. Figure 2 illustrates the interfaces and the flow velocities in the basic state for the isolated front.

*c. The perturbation equations*

We superimpose small wavelike perturbations of the form

$$(\hat{u}, \hat{v}, \hat{p}) = (u'(y), v'(y), p'(y))e^{i(\kappa x - \omega t)} \tag{13}$$

on the basic flow, where $\omega$ is complex frequency and $\kappa$ is wave number. The linearized perturbation equations expressed in terms of pressure variables are, in *Zone II* (Lee, 1993):

$$\left(\frac{\bar{h}_1}{Q_1}\right)\frac{d^2p'_1}{dy^2} + \left(\frac{\bar{h}_1}{Q_1}\right)_y \frac{dp'_1}{dy} - \left[\frac{\kappa}{(\bar{u}_1\kappa - \omega)}\left(\frac{\bar{h}_1}{Q_1}\right)_y + \kappa^2\left(\frac{\bar{h}_1}{Q_1}\right)\right]p'_1 = (p'_1 - p'_2), \tag{14}$$

$$\left(\frac{\bar{h}_2}{Q_2}\right)\frac{d^2p'_2}{dy^2} + \left(\frac{\bar{h}_2}{Q_2}\right)_y \frac{dp'_2}{dy} - \left[\frac{\kappa}{(\bar{u}_2\kappa - \omega)}\left(\frac{\bar{h}_2}{Q_2}\right)_y + \kappa^2\left(\frac{\bar{h}_2}{Q_2}\right)\right]p'_2 = \frac{(1+\alpha)}{\alpha\delta}p'_2 - \frac{1}{\delta}p'_1 - \frac{1}{\alpha\delta}p'_3, \tag{15}$$

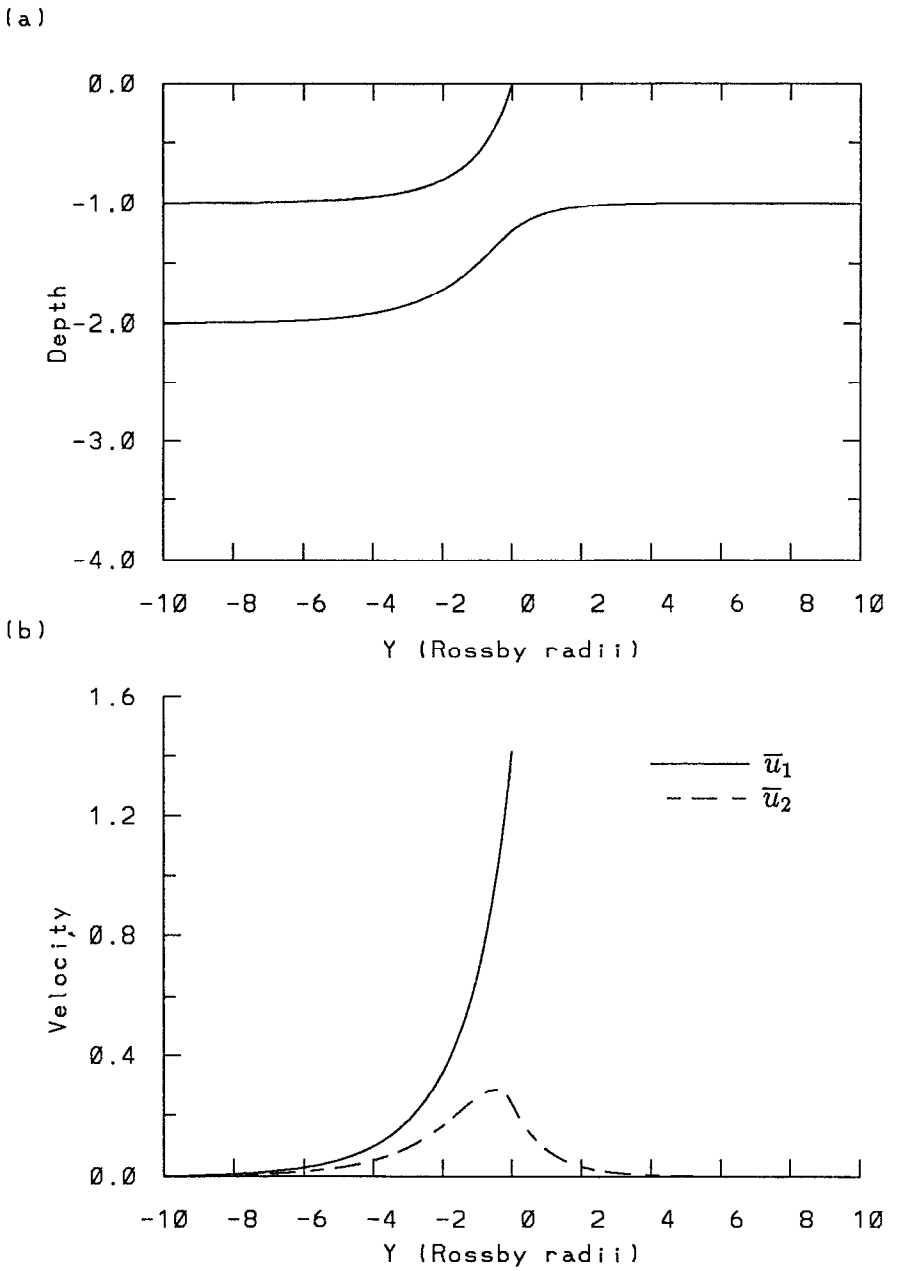


Figure 2. Basic geostrophic flow of the isolated front: (a) Layer thickness, (b) Velocity when $\alpha = 1, \delta = 1$ and $\gamma = 8$.

$$\frac{d^2p'_3}{dy^2} - \left[\frac{\bar{h}_{1y} + \delta\bar{h}_{2y}}{(\gamma - \bar{h}_1 - \delta\bar{h}_2)}\right]\frac{dp'_3}{dy} - \left[\kappa^2 + \frac{(\bar{h}_{1y} + \delta\bar{h}_{2y})\kappa}{\omega(\gamma - \bar{h}_1 - \delta\bar{h}_2)}\right]p'_3 = -\frac{(\omega^2 - 1)}{\alpha(\gamma - \bar{h}_1 - \delta\bar{h}_2)}(p'_3 - p'_2), \tag{16}$$

where

$$Q_j = \left(1 - \frac{d\bar{u}_j}{dy}\right) - (\bar{u}_j\kappa - \omega)^2, \qquad j = 1, 2. \tag{17}$$

In *Zone I,* the equations reduce to:

$$\left(\frac{\bar{h}_2}{Q_2}\right)\frac{d^2p'_2}{dy^2} + \left(\frac{\bar{h}_2}{Q_2}\right)_y\frac{dp'_2}{dy} - \left[\frac{\kappa}{(\bar{u}_2\kappa - \omega)}\left(\frac{\bar{h}_2}{Q_2}\right)_y + \kappa^2\left(\frac{\bar{h}_2}{Q_2}\right)\right]p'_2 = \frac{1}{\alpha\delta}(p'_2 - p'_3), \tag{18}$$

$$\frac{d^2p'_3}{dy^2} - \left[\frac{\delta\bar{h}_{2y}}{(\gamma - \delta\bar{h}_2}\right]\frac{dp'_3}{dy} - \left[\kappa^2 + \frac{\delta\bar{h}_{2y}\kappa}{\omega(\gamma - \delta\bar{h}_2)}\right]p'_3 = -\frac{(\omega^2 - 1)}{\alpha(\gamma - \delta\bar{h}_2)}(p'_3 - p'_2). \tag{19}$$

The three equations in *Zone II* and two in *Zone I* are the equations to be integrated, with boundary conditions representing: (i) an isolated front, (ii) a coastal front.

*d. Boundary conditions*

For the isolated front, at $y = \pm\infty$ all perturbations vanish:

$$p'_1(y) = p'_2(y) = p'_3(y) = 0, \qquad \text{at} \qquad y = \pm\infty. \tag{20}$$

At $y = 0$, where the front intersects the surface, five boundary conditions must be satisfied: a kinematic boundary condition at $y = 0$ expressing continuity of the free surface plus the continuity of pressure and velocity of the second and third layers. The kinematic condition is:

$$\frac{Dy_f}{Dt} \simeq i(\bar{u}_1\kappa - \omega)y_f = \hat{v}_1 \qquad \text{at} \qquad y = 0 \tag{21}$$

where $y_f$ is the horizontal displacement of the front. To first order in the small quantity $y_f$, this is equivalent to

$$i\frac{d\bar{h}_1}{dy}v'_1 - h'_1(\bar{u}_1\kappa - \omega) = 0 \qquad \text{at} \qquad y = 0. \tag{22}$$

The result also follows directly from the continuity equation for the top layer, with $\bar{h}_1(0) = 0$. Reduced to pressure variables, the result is:

$$\frac{dp'_1}{dy}(0) + \left[\frac{(\bar{u}_1(0)\kappa - \omega)^2}{\bar{h}_{1y}(0)} - \frac{\kappa}{\bar{u}_1(0)\kappa - \omega)}\right]p'_1(0) - \frac{(\bar{u}_1(0)\kappa - \omega)^2}{\bar{h}_{1y}(0)}p'_2(0) = 0. \tag{23}$$

The continuity of pressure of the second layer is

$$p_2^{II}(y_f) = p_2^I(y_f) \tag{24}$$

where superscripts *I*, *II* indicate *Zone I* and *Zone II* respectively. A Taylor expansion of $p_2^{II}(y_f)$ about $y = 0$, after linearization, gives

$$p_2^{II}(y_f) = y_f \frac{d\bar{p}_2^{II}}{dy}(0) + \bar{p}_2^{II}(0) + p_2^{II\prime}(0). \tag{25}$$

Similarly, for $p_2^I(y_f)$ we get

$$p_2^I(y_f) = y_f \frac{d\bar{p}_2^I}{dy}(0) + \bar{p}_2^I(0) + p_2^{I\prime}(0). \tag{26}$$

Using the continuity of pressure and the pressure gradient of the basic flow at $y = 0$, we get from the last three equations

$$p_2^{II\prime}(0) = p_2^{I\prime}(0). \tag{27}$$

The continuity of surface elevation:

$$\eta_1^{II}(y_f) = \eta_2^I(y_f) \tag{28}$$

gives the same boundary condition as we found from the continuity of second layer pressure, because $p_1(y_f) = p_2(y_f)$ at $y = y_f$ where $h_1 = 0$. The continuity of third layer pressure gives

$$p_3^{II\prime}(0) = p_3^{I\prime}(0). \tag{29}$$

Finally, the continuity of cross-frontal velocity in the second and third layers, after linearization, gives

$$v_2^{II\prime}(0) = v_2^{I\prime}(0) \tag{30}$$

$$v_3^{II\prime}(0) = v_3^{I\prime}(0) \tag{31}$$

since the basic state cross-front velocity is zero everywhere. In terms of pressure variables those conditions yield:

$$\frac{dp_2^{II\prime}}{dy}(0) = \frac{dp_2^{I\prime}}{dy}(0), \tag{32}$$

$$\frac{dp_3^{II\prime}}{dy}(0) = \frac{dp_3^{I\prime}}{dy}(0). \tag{33}$$

Summarized, the five boundary conditions at $y = 0$, written in terms of the pressure,

are:

$$\frac{dp'_1}{dy}(0) + \left[\frac{(\bar{u}_1(0)\kappa - \omega)^2}{\bar{h}_{1y}(0)} - \frac{\kappa}{(\bar{u}_1(0)\kappa - \omega)}\right]p'_1(0) - \frac{(\bar{u}_1(0)\kappa - \omega)^2}{\bar{h}_{1y}(0)}p_2(0)' = 0,$$

$$\begin{aligned} p_2^{II\prime}(0) &= p_2^{I\prime}(0), \\ p_3^{II\prime}(0) &= p_3^{I\prime}(0), \\ \frac{dp_2^{II\prime}}{dy}(0) &= \frac{dp_2^{I\prime}}{dy}(0), \\ \frac{dp_3^{II\prime}}{dy}(0) &= \frac{dp_3^{I\prime}}{dy}(0). \end{aligned} \tag{34}$$

Together with the five boundary conditions at infinity, we now have a total of 10 boundary conditions for 5 second order ODEs.

## 3. Method of solution

At infinity, the perturbation equations 12 to 16, 18 and 19 reduce to homogeneous, constant coefficient ordinary differential equations for the three pressure variables in *Zone II,* two in *Zone I.* The three equations applying at negative infinity can be satisfied by exponential solutions of the form $A\ \exp(ky)$, where $k$ satisfies a third degree algebraic equation, the determinant of the matrix of coefficients set equal to zero. Each of the three roots $k_i$ yields amplitude ratios between the pressure variables $p'_j$ with one amplitude remaining arbitrary. The total solution is then of the form:

$$\begin{aligned} p'_1 &= A_a p_{1a} + A_b p_{1b} + A_c p_{1c}, \\ p'_2 &= A_a p_{2a} + A_b p_{2b} + A_c p_{2c}, \end{aligned} \tag{35}$$

$$p'_3 = A_a p_{3a} + A_b p_{3b} + A_c p_{3c}, \tag{36}$$

where $A_a, A_b$ and $A_c$ are yet to be determined, but the $p'_{il}$ are fully defined exponential functions for given $\kappa$ and $\omega$, of the same $e$-folding scale of $k^{-1}$ for the same letter index.

Similarly, at $y \to +\infty$, the solutions which satisfy boundary conditions:

$$p'_2 = p'_3 = 0, \quad \text{at } y \to +\infty, \tag{37}$$

are pairs of simple exponential solutions, which we may write as

$$p'_2 = B_p p_{2p} + B_m p_{2m}, \tag{38}$$

$$p'_3 = B_p p_{3p} + B_m p_{3m} \tag{39}$$

where $B_p$ and $B_m$ are also yet to be determined.

We integrated equations (12–16, 18, 19) numerically using a fourth-order Runge-Kutta scheme. The analytical solutions at $y \to \pm\infty$ (Eqs. 35 and 37) were used as initial conditions and the solutions were marched from $y = \pm\infty$ (practically $y = \pm 10$) to $y = 0$, with a trial complex eigenvalue $\omega$ and a fixed wave number $\kappa$. Three nondimensional parameters $\alpha$, $\delta$, and $\gamma$ specifying the physical characteristics of the front were also prescribed.

The five constants $A_a$ to $A_c$, $B_p$ and $B_m$ were determined from the matching conditions at $y = 0$. Those conditions, (Eqs. 34), are in matrix form,

$$\begin{bmatrix} F_a & F_b & F_c & 0 & 0 \\ p_{2a} & p_{2b} & p_{2c} & -p_{2p} & -p_{2m} \\ p_{2ya} & p_{2yb} & p_{2yc} & -p_{2yp} & -p_{2ym} \\ p_{3a} & p_{3b} & p_{3c} & -p_{3p} & -p_{3m} \\ p_{3ya} & p_{3yb} & p_{3yc} & -p_{3yp} & -p_{3ym} \end{bmatrix} \begin{bmatrix} A_a \\ A_b \\ A_c \\ B_p \\ B_m \end{bmatrix} = 0 \tag{40}$$

where $F_a$, $F_b$ and $F_c$ are defined as follows:

$$F_a = p_{1ya}(0) + \left[\frac{(\bar{u}_1(0)\kappa - \omega)^2}{\bar{h}_{1y}(0)} - \frac{\kappa}{(\bar{u}_1(0)\kappa - \omega)}\right] p_{1a}(0) - \frac{(\bar{u}_1(0)\kappa - \omega)^2}{\bar{h}_{1y}(0)} p_{2a}(0), \tag{41}$$

$$F_b = p_{1yb}(0) + \left[\frac{(\bar{u}_1(0)\kappa - \omega)^2}{\bar{h}_{1y}(0)} - \frac{\kappa}{(\bar{u}_1(0)\kappa - \omega)}\right] p_{1b}(0) - \frac{(\bar{u}_1(0)\kappa - \omega)^2}{\bar{h}_{1y}(0)} p_{2b}(0), \tag{42}$$

$$F_c = p_{1yc}(0) + \left[\frac{(\bar{u}_1(0)\kappa - \omega)^2}{\bar{h}_{1y}(0)} - \frac{\kappa}{(\bar{u}_1(0)\kappa - \omega)}\right] p_{1c}(0) - \frac{(\bar{u}_1(0)\kappa - \omega)^2}{\bar{h}_{1y}(0)} p_{2c}(0). \tag{43}$$

The determinant of the matrix must vanish in order for nontrivial eigenfunctions to exist: this yields an equation for the calculation of the complex eigenvalue $\omega$ for chosen $\kappa$. The matrix contains the values of eigenfunctions at $y = 0$. These were obtained from the numerical integrations, and then used to calculate the determinant. The trial eigenvalue $\omega$ was corrected using Muller's method (Gerald and Wheatly, 1984). The procedure was repeated until the value of the determinant reduced to order $10^{-8}$. The matching conditions then allowed the determination of the constants $A_a$ to $A_c$, $B_p$ and $B_m$, except that one remained arbitrary. The combined eigenfunctions could now be determined, put together on the scheme of Eqs. 35 and 37 but now for the entire $y$-domain. The same calculations were carried out for the coastal front, mutatis mutandis.

## 4. Calculated results

### a. Structure and properties of the instability waves

We chose for our calculations parameters typical of the Gulf Stream west of 73W. The layer thicknesses are $H_1 = 500$ m, $H_2 = 500$ m and $H_T = 4000$ m. These yield $\delta = 1$ and $\gamma = 8$. The mean densities ($\sigma_t$) in the three layers of 26.90, 27.30 and 27.70 give $\alpha = 1.0$ and the internal Rossby radius $R_d$ ($=\sqrt{g\epsilon_{21}H_1}f^{-1}$) is approximately 30 km. The layer thicknesses determine potential vorticity and hence the mean flow. This choice of parameters serves as a standard case with which the results of the model with different parameter values may be compared.

*i. Isolated front.* We found solutions for a range of alongfront wavenumbers $\kappa$ and determined the complex frequency $\omega = \omega_r + i\omega_i$, as a function of $\kappa$, see Figure 3. The growth rate $\omega_i$ has a maximum nondimensional value $\omega_{im}$ of 0.0274 at $\kappa = 0.43$. The frequency $\omega$ is purely real above the critical wavenumber $\kappa_c \simeq 0.59$ where $\omega_i = 0$. The values of $\omega_r$ are all positive and the phase speed, which is defined as $c = \omega_r/\kappa$, is also positive, so that the wave propagates downstream. The positive 2nd derivative of the $\omega_r(\kappa)$ curve implies that the wave is dispersive with positive group velocity so that the energy of the wave also propagates in the downstream direction.

The dimensional properties of the most unstable wave are as follows. The length scale $R_d$ is approximately 30 km for the "typical" case. The wavelength of the most unstable wave is therefore 483 km. The $e$-folding time scale is 4.2 days, the phase speed of 19 cm s$^{-1}$ showing that the wave propagates downstream very slowly compared with the mean flow speed.

The structure of the most unstable wave is illustrated in Figure 4 and 5. The amplitude of $p'_1$ was taken to be unity (this is the one remaining arbitrary constant, see previous discussion). Figure 4 shows the distribution of pressure and velocity amplitude, Figure 5 the two-dimensional pattern of the eigenfunctions. The wavy line shows the displacement of the front, for orientation in comparing phases. Contour lines show pressure, arrows velocity vectors.

We also examined the effect of varying the parameter $\gamma$, the ratio of bottom layer to top layer depth. Increasing the value of $\gamma$ reduces the growth rate and shifts the maximum growth rate to lower wavenumber (as found by Killworth *et al.*, 1984). As the bottom layer thickness increases compared to the upper two layers, the shear between the lower two layers decreases, and with it the growth rate (a point also made by Barth, 1987).

*ii. Coastal front, flat bottom.* The width of the two layer zone $y_c$ was chosen to be six times the Rossby radius, other parameters the same as for the isolated front. The maximum growth rate was 0.0182 at $\kappa_m = 0.49$, considerably less than for the isolated front. We obtained a dimensional wavelength for the most unstable wave of 385 km, an $e$-folding time scale of 6.3 days and a phase speed of 19.2 cm s$^{-1}$. The wave is less unstable, the wavelength of the most unstable wave slightly shorter, than for the

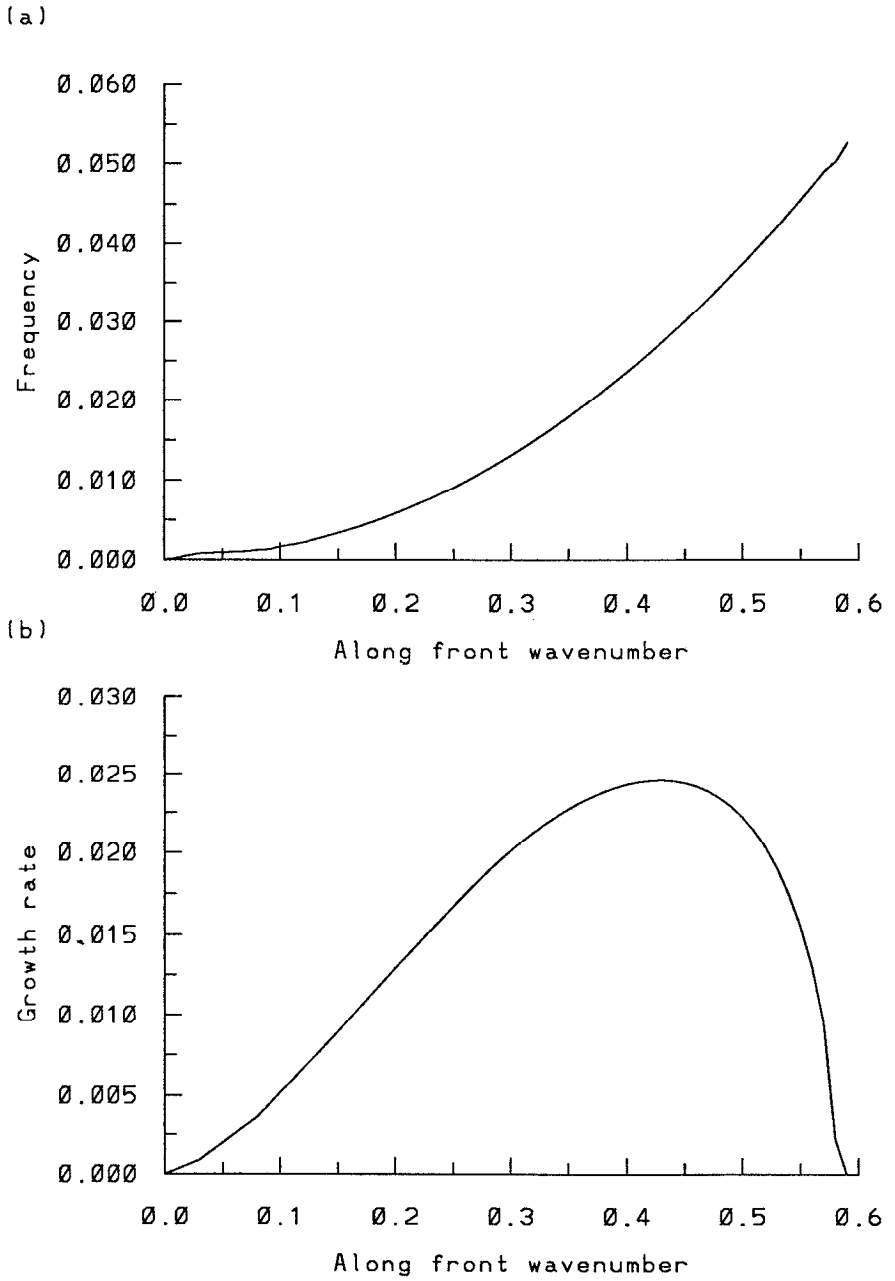


Figure 3. Isolated front: (a) Frequency of the fastest growing wave as a function of along front wave number $\kappa$, (b) Growth rate of the fastest growing wave as a function of along front wave number $\kappa$.

isolated front. The calculation was carried out again for several values of $y_c$. The growth rate remains almost the same as for $y_c = 6$ except when $y_c$ is one or less. Oey (1988) found from a numerical study that the growth rate of frontal instabilities in a coastal region depends primarily on nondimensional width of the coastal region ($y_c$ in this study). He also found that for $y_c > 1$, increasing $y_c$ neither stabilizes nor destabilizes the flow. However, when $y_c < 1$, the growth rate does decrease rapidly as the coastal wall interferes with cross-front motions.

*iii. Coastal front, sloping bottom.* Since most oceanic fronts are located near coasts, the dynamical effects of sloping bottom topography are of interest. The influence of bottom topography on frontal instability was first studied by Orlanski (1969). He used a hyperbolic-tangent function for the shape of the bottom and bound a destabilizing effect. Recently, Barth (1987) used a set of approximate equations with linear bottom topography and found a stabilizing effect of the bottom, opposite to Orlanski's result.

Here we used a hyperbolic tangent function for the shape of the bottom similar to Orlanski's (1969):

$$h_B = H_0\left(\tanh\frac{1}{2}(y + 1) + 1\right) \tag{44}$$

where $H_0$ is the bottom depth $h_B$ at $y = y_c$, chosen to be 3. The distance to the coast, $y_c$ is six times the Rossby radius, the rest of the parameters the same as for the flat bottom model. The maximum growth rate is now 0.0415 at $\kappa_m = 0.60$. The dimensional wavelength of the most unstable wave is about 314 km, the $e$-folding time scale of 2.8 days and the phase speed of 33.7 cm $s^{-1}$. Compared with the flat bottom case, the wave is more unstable, the wavelength of the most unstable wave shorter, the phase speed greater. The eigenfunctions of the fastest growing wave are, however, not very different (Lee, 1993). Calculations were also made for $H_0 = 2, 4$. The results show that steeper bottom topography destabilizes the front, and the wavelength of the most unstable wave decreases as the slope of the bottom topography increases.

### b. *Inferences on thermocline motions*

In order to visualize the effects of an instability wave on a separated boundary current it is necessary to combine the basic state with the flow perturbation. Starting with a streamwise velocity perturbation equal to one percent of the peak basic flow velocity (isolated front) we allowed the perturbation to grow for a full period, by which time the wave amplitude (displacement of the surface front) was about 10% of the wavelength, and added this to the basic flow. This still qualifies as small amplitude, while clearly portraying the wave motion. Figure 6 shows the perturbed flow in the thermocline layer: solid lines are pressure contours, arrows velocities, dotted line surface front shape. In general, thermocline flow follows the surface layer flow. Departures are greatest near the inflection points of the streamlines: upstream

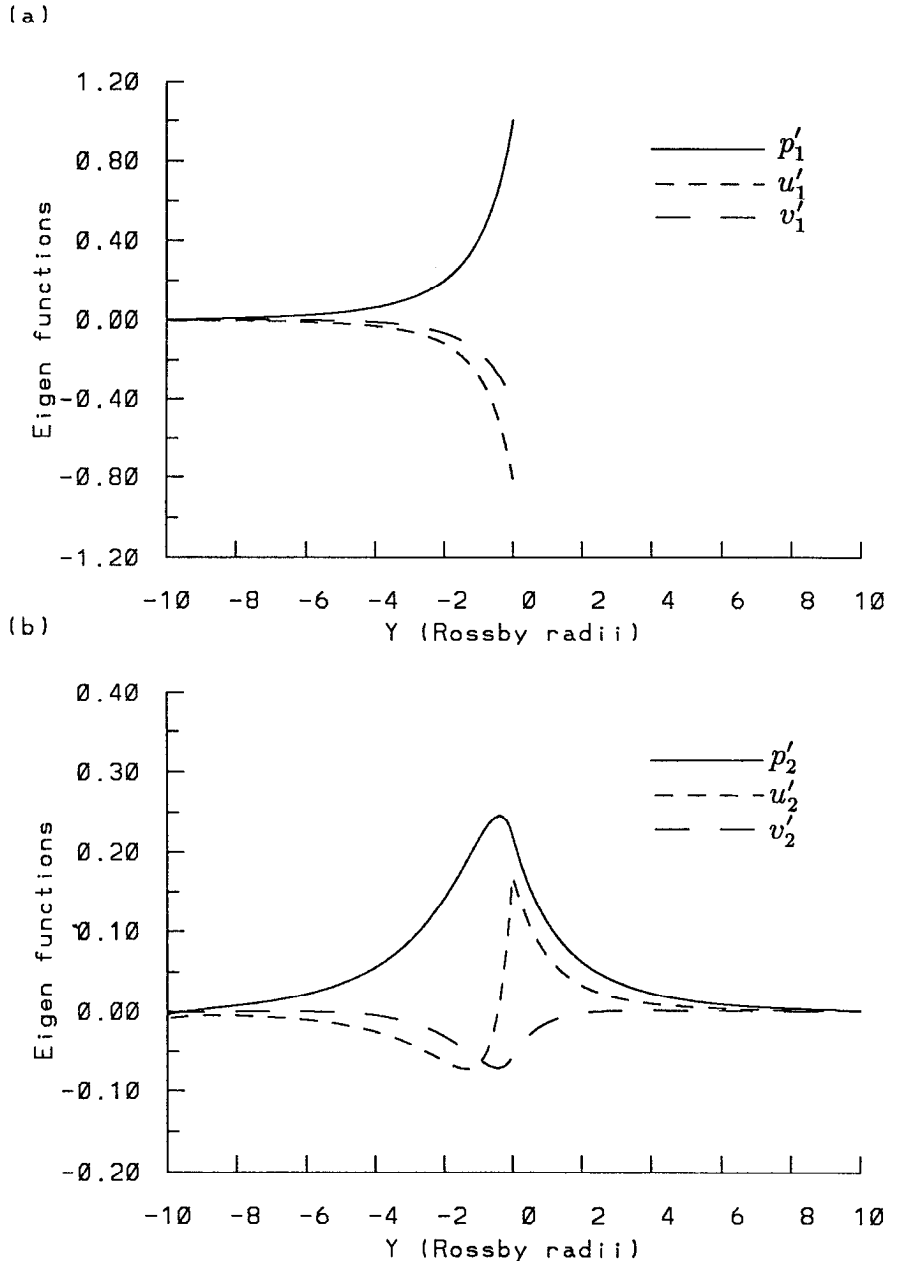


Figure 4. Isolated front: Eigenfunctions of the most unstable wave of (a) the top layer, (b) the thermocline layer and (c) the bottom layer.

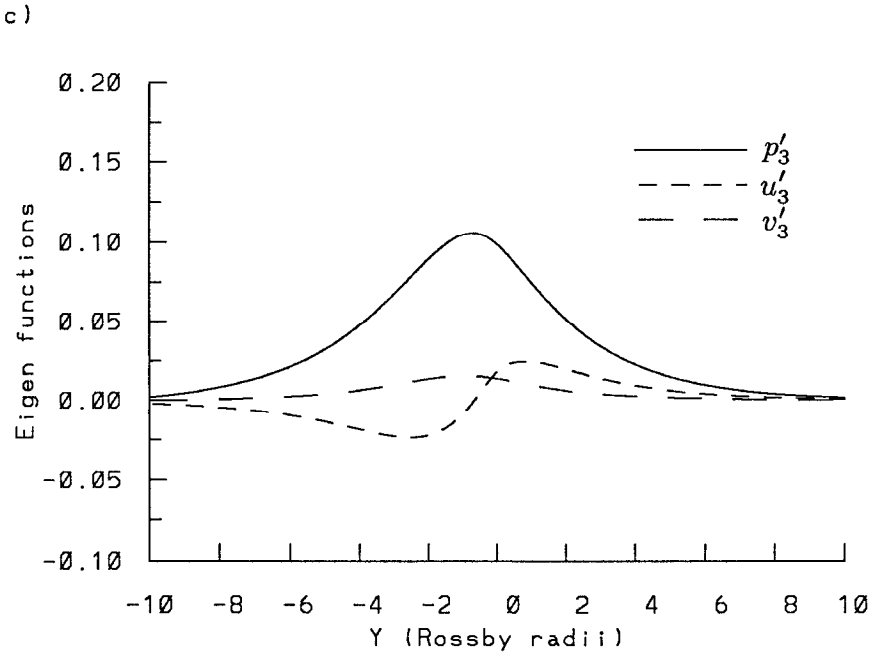


Figure 4. (Continued)

of a trough there is marked inflow from the coastal side of the current, outflow upstream of a crest. While the velocity-anomalies (compared to the surface velocities) are small, they involve enough fluid to generate closed streamlines (pressure contours, strictly speaking, but the differences are small) in "slope-water," on the coastal side of the current, forming a weak cyclonic eddy in the trough of the wave. There is no anticyclonic eddy over the crest, nor a comparable flow structure on the deep side of the current. We have also calculated particle trajectories of the combined flow, starting the particles in the core of the basic current. Results are shown in Figure 7. The wavelength is about 15 $R_d$, so that at the end of one wavelength's worth of travel some of the particles leave the current for the coastal side, all of them by the end of another wave. Note that the particles always leave just after completing a cyclonic turn (as they come out of a trough). As Figure 6 has shown, this is where they acquire a shoreward pointing velocity anomaly. The large cross-stream displacements seen in Figure 7 of course occur at finite perturbation amplitude and should not be taken seriously.

*c. Comparison with observation*

As we have emphasized before, small amplitude instability wave theory only tells us how the large meanders on a boundary current may start, with hope but no guarantee that finite amplitude motions will have a structure similar to the eigenfunc-

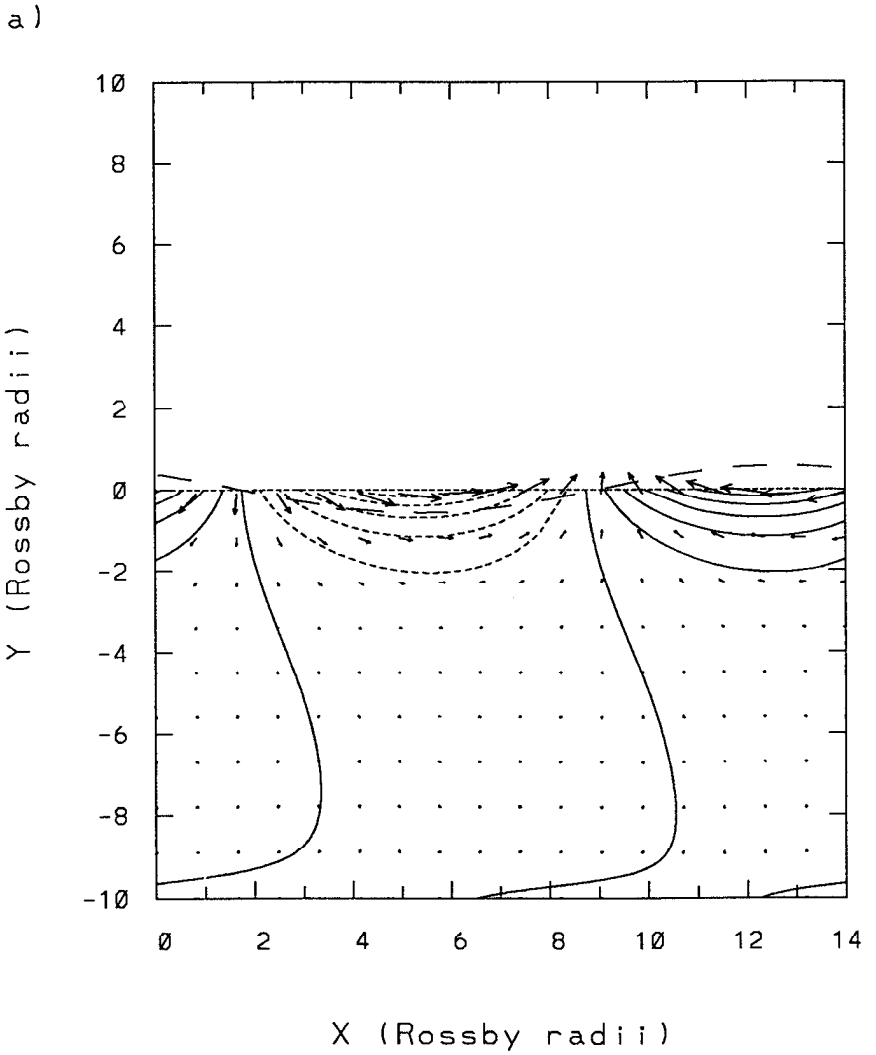


Figure 5. Isolated Front: Two-dimensional structure of the eigenfunctions (contours of pressure and velocity vectors), (a) the top layer, (b) the thermocline layer, (c) the bottom layer. The solid and dashed lines indicate positive and negative contours, and the wavy line the phase of the surface front displacement. Contour intervals and magnitudes are not regular for each figures. To compare relative magnitudes, see Figure 4.

tions. Compounding the problem of model-observation comparison is the overidealized character of the model: a single "thermocline" layer is a poor surrogate for the onion-skin arrangement of many isopycnal layers in the main oceanic thermocline. Nevertheless, the layers in the Gulf Stream thermocline in contact with slopewater

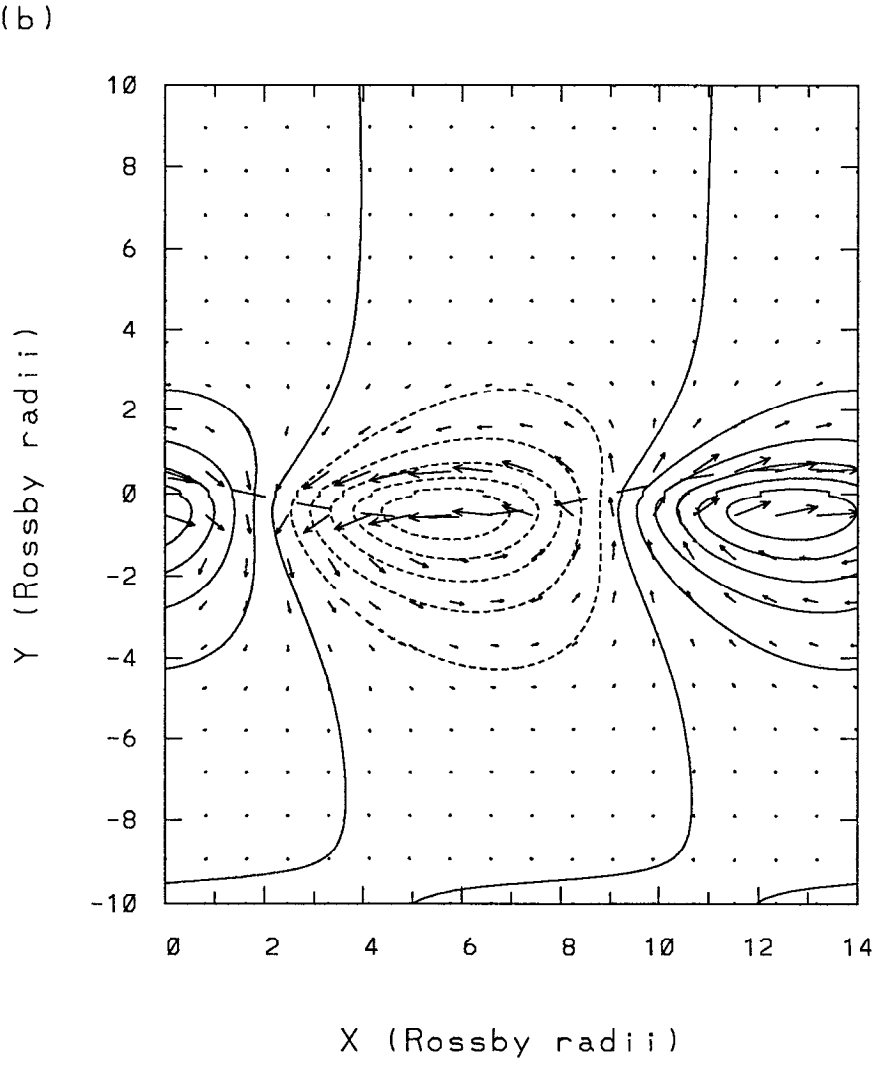


Figure 5. (Continued)

are a subset subject to similar boundary conditions, and might just behave as the theory suggest.

On wavelength, phase speed and growth rate, the thorough analysis of observations by Watts and Johns (1982) is probably the best source of information. There are considerable difficulties in separating the behavior of different-length unstable waves, and the results are subject to uncertainty, according to Watts and Johns, of 25% on wavelength and phase speed, to 100% on $c_i$. The best estimate on the wavelength of the most unstable wave seems to be near 400 km, judged from their

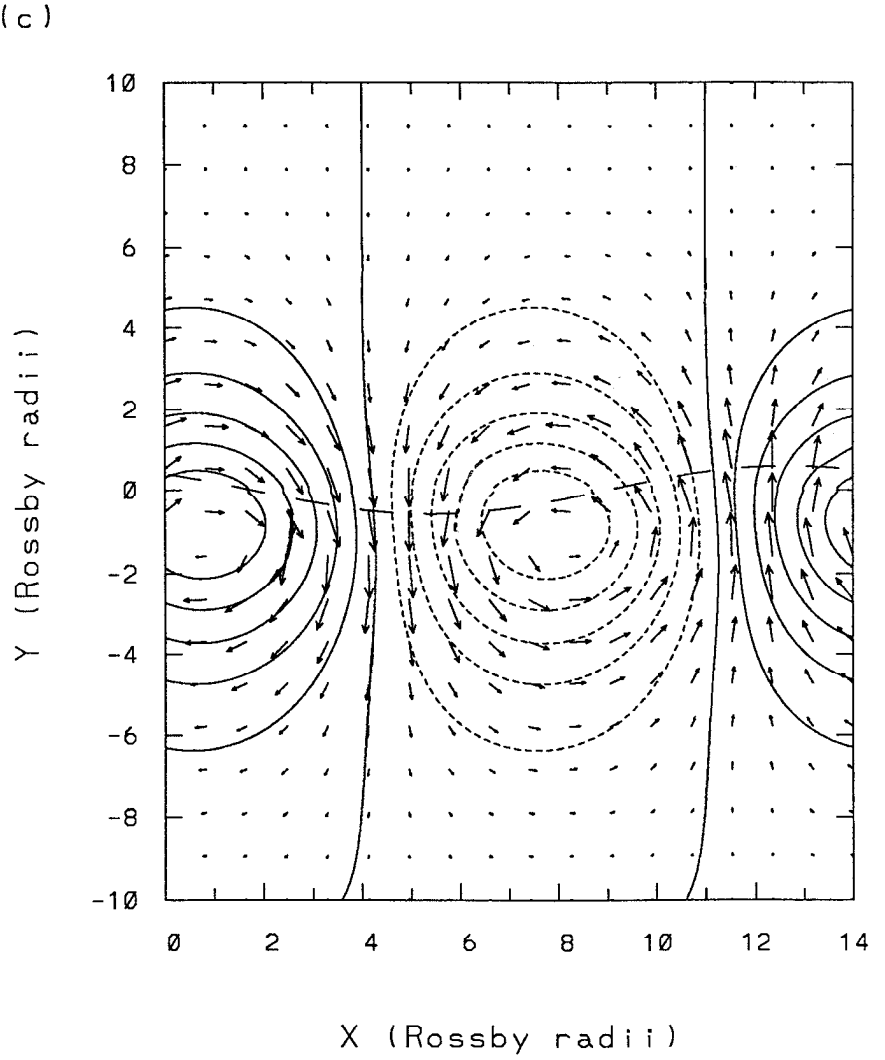


Figure 5. (Continued)

Figures 10a and 10b. The phase speed of this wave is estimated to be 0.3 m $s^{-1}$, from the same figures, the *e*-folding time scale 6 days. Our standard model yielded calculated results of 438 km wavelength, phase speed of 0.19 m $s^{-1}$, and an *e*-folding time scale of 4.2 days. In view of the uncertainty of the values derived from observation, and of the overidealized nature of the model, one could hardly expect better agreement.

A much stricter test of the theory, and more important from the point of view of our objective of elucidating mass exchange between slopewater and the Gulf Stream

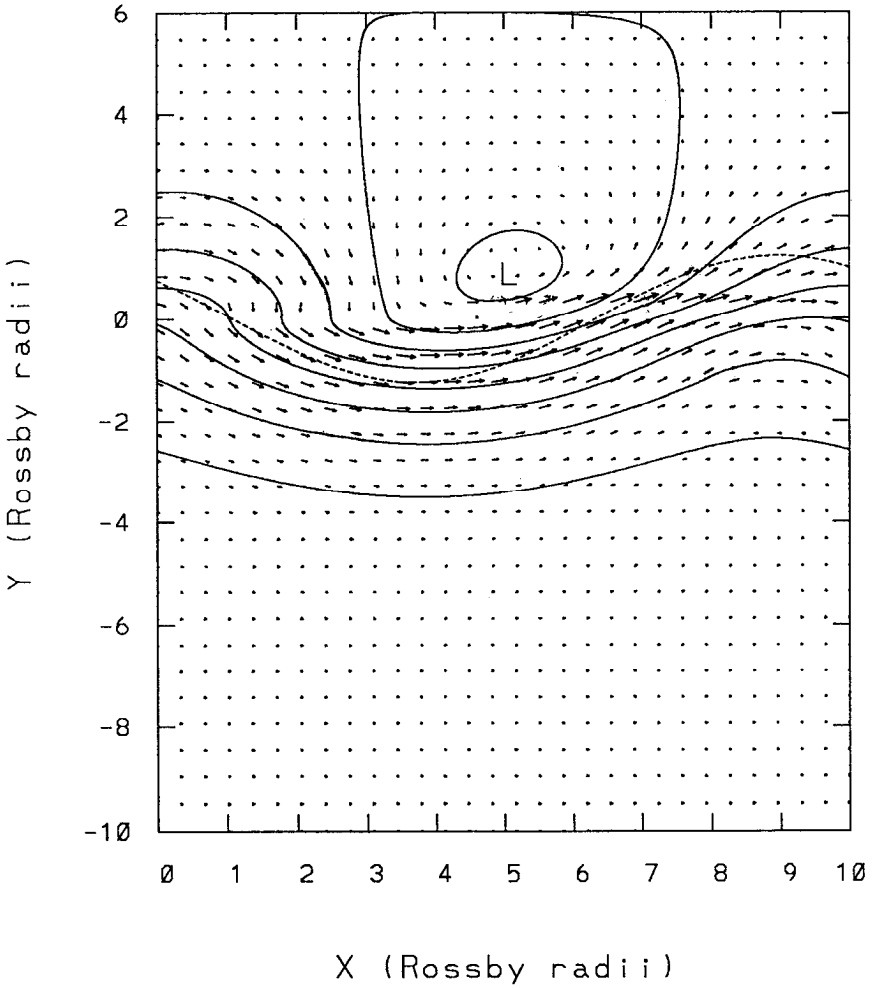


Figure 6. Contours of total pressure and total velocity vectors (basic flow plus perturbations) in the thermocline layer (coastal front, sloping bottom when $H_0 = 3$). Dashed lines show the evolution of perturbed front $y_f$.

thermocline, is a comparison with thermocline motions, observed recently by Rossby and his collaborators (see Bower and Rossby, 1989 and references given there) using RAFOS floats. These floats follow isopycnal surfaces to a good approximation. Released into the thermocline, in the core of the current, they follow the meanders of the Stream, with some characteristic departures: they move shoreward and upward on the isopycnal surfaces as they approach a meander crest, seaward and downward approaching a trough. This is exactly what our combined basic-perturbation flow (Fig. 6) showed. Bower and Rossby also point out that the floats eventually escape from the Stream. We show here one illustration from Bower *et al.*

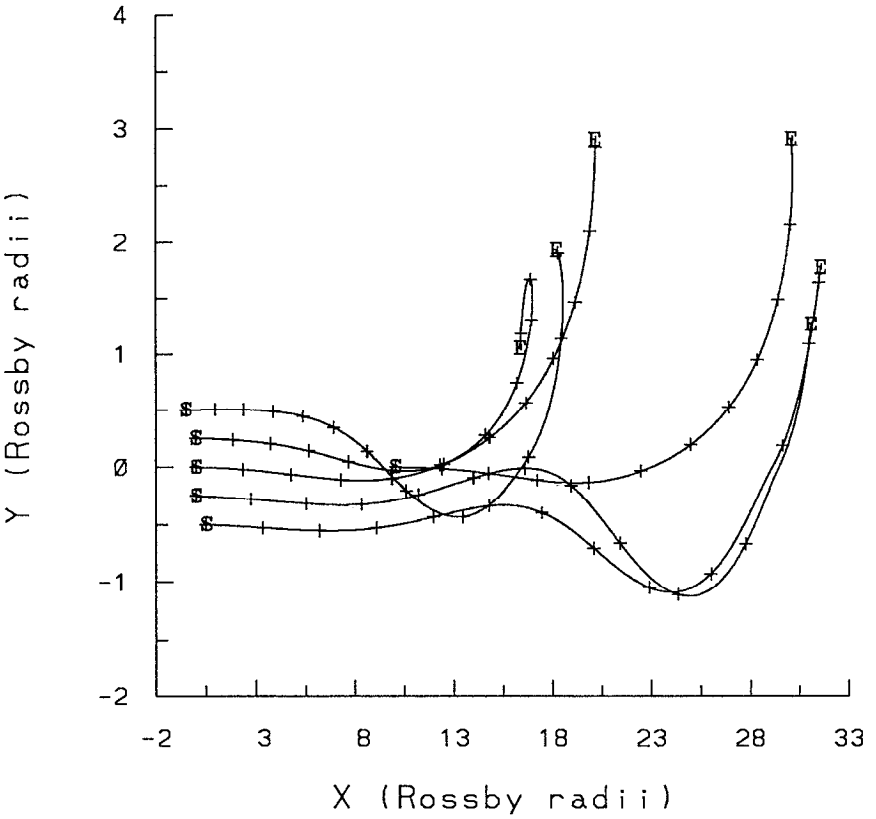


Figure 7. Trajectories of particles in the thermocline layer initially located at the point 'S'. An 'E' sign indicates the ending point. A '+' sign is placed at each time step.

(1986), the path of RAFOS 052, see Figure 8. The numbers on the path identify Julian days. The float meandered along with the Stream to about day 290, when it was about at the crest of a meander (according to its pressure-history, not shown here). From here it did not return to its original cross-stream location but escaped to slopewater, there moving slowly southwestward from day 300 on, at a constant depth. As in our particle simulation, the escape came after entering the anticyclonic motion in the crest of a meander.

There are other complexities in the observed float motions which our simple model did not simulate: for example, floats also escaped on the deep, seaward, side of the Stream. Nevertheles, the key features of the calculated thermocline motions agree with observation: flow in the thermocline layer follows the surface layer closely, except for slightly exaggerated shoreward motion upon approaching a meander crest, seaward motion anomaly entering a trough. Escape from the current is a finite amplitude phenomenon, not well simulated by the model, although the velocity anomalies hint at this, too.

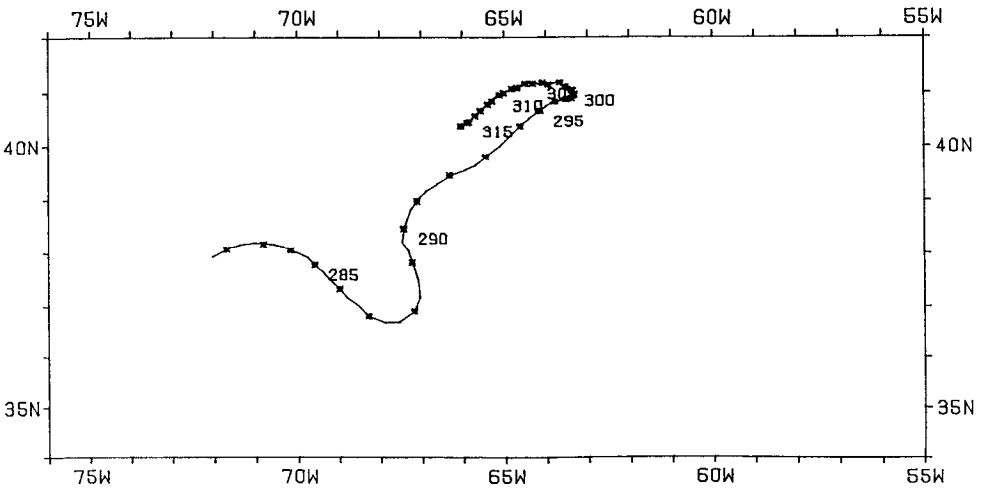


Figure 8. RAFOS float trajectories on 10°C surface ($\sigma_t$ = 27.2). Dots on the trajectory are 0000 UTC fixes and dates are yeardays in 1984. Reproduced from Bower *et al.* (1986).

Our reviewers insisted that we acknowledge previous attempts at interpreting RAFOS float observations in terms of Gulf Stream models by Garvine (1988) and Cushman-Roisin (1993). Both these authors used one-and-a-half layer models, Garvine an earlier instability wave theory of his own (Garvine, 1984) similar to Paldor's (1983), Cushman-Roisin a finite amplitude quasi-geostrophic jet model. Both approximate thermocline motions by those of particles at the bottom of their surface (only) active layer. Because the surface layer terminates at the outcrop of the front, such particles cannot move beyond the front. Their horizontal motion is identical with surface motion. So long as thermocline layers follow surface layer motion, the results of Garvine and Cushman-Roisin are valid, to the extent their models are. The important question here is, however, how far thermocline motion departs from surface motion, to allow the exchange of fluid between submerged portions of the thermocline with surface fluid shoreward of the current.

## 5. Summary

The primary objective of this study was to gain insight into the behavior of the thermocline layer in an unstable, separated boundary current. The eigenfunctions of the most unstable wave show a cyclonic thermocline eddy underlying the trough of a meander, an anticyclonic eddy the crest. Putting mean flow and perturbation together, a large cyclonic eddy (some 200 km diameter) develops in slopewater, shoreward of a meander trough. The dominant feature of calculated particle trajectories in the thermocline layer is ejection into slopewater. Of course linear instability calculations can only suggest tendencies in the finite-amplitude development of geostrophic turbulence. Nevertheless, the large range of unstable thermo-

cline eddy motion strongly suggests vigorous exchange between slopewater and the Gulf Stream thermocline, as inferred from observation. We found, however, no support for the idea that the observed acceleration of the upper slope current in the Mid-Atlantic Bight at the time of Gulf Stream approach to the coast is due to motion in the thermocline layer opposite to the surface layer: thermocline motions largely follow surface motion.

On the more conventional topic of Gulf Stream instability, our three layer model revealed unstable ageostrophic perturbations of fairly long wavelength. For parameters typical of the Gulf Stream west of 70W, the most unstable wave was found to propagate slowly in the downstream direction with a phase speed of 19–33.7 cm $s^{-1}$, an *e*-folding time scale of 2.8–6.3 days and a wavelength of 314–438 km. These values compare well with unstable wave characteristics deduced from observation by Watts and Johns (1982).

Calculations of energy conversion (see appendix) rates revealed that the unstable waves of the boundary current grew mainly on account of baroclinic instability, the effect of horizontal shear being relatively minor, the Reynolds stress extracting energy from the mean flow.

Regarding the effect of an active thermocline layer on the instability, the growth rate was slightly less, the wavelength of the most unstable wave much greater than for the two-layer case. An active thermocline layer thus slightly stabilizes the front and shifts the instability to lower wavenumber. We also found that confining the two-layer region by a coast stabilizes the front, but only when the width drops below an internal deformation radius, a result previously obtained by Oey (1988). Finally, the results showed that the bottom topography (of hyperbolic-tangent shape) destabilizes the front.

*Acknowledgments.* The first author would like to thank Dr. Glen Wheless and Dr. Chet Grosch for valuable comments on the manuscript. Computer resources and facilities were provided by the Commonwealth Center for Coastal Physical Oceanography.

## APPENDIX

### The physical mechanism of the instability

Geostrophic fronts, particularly those associated with the western boundary currents, have been long recognized as huge reservoirs of potential energy. Theoretical studies have shown that geostrophic fronts have ratios of available kinetic energy to potential energy of approximately 1:3 (Gill, 1982; Ou, 1986; Van Heijst, 1985), and that they are prone to baroclinic instability. In addition, the front is usually accompanied by large horizontal velocity shear which may be the energy source for barotropic instability. Therefore, both energy transformation mechanisms may be simultaneously present in a geostrophic front (Fedorov, 1986). Here we calculate energy transformations in our model to determine the primary source of energy for the unstable waves.

*a. Wave energy equations.* The wave energy equation can be obtained directly from the linearized governing equations (Pedlosky, 1987). The equations for the wave energies integrated over the entire domain (one wavelength in $x$, from $y = -\infty$ to $+\infty$ for the isolated front and from $y = -\infty$ to $y_c$ for the coastal front) are

$$\begin{aligned}\frac{\partial K_w}{\partial t} &= \frac{\partial}{\partial t}\int_s \left[\bar{h}_1 \frac{(\hat{u}_1^2 + \hat{v}_1^2)}{2} + \delta\bar{h}_2 \frac{(\hat{u}_2^2 + \hat{v}_2^2)}{2} + \bar{h}_3 \frac{(\hat{u}_3^2 + \hat{v}_3^2)}{2}\right] ds \\ &= -C(K_w \to K_m) - C(K_w \to P_w),\end{aligned} \tag{A1}$$

$$\frac{\partial P_w}{\partial t} = \frac{\partial}{\partial t}\int_s \left[(1+\alpha)\frac{\hat{h}_1^2}{2} + \alpha\delta^2 \frac{\hat{h}_2^2}{2} + \alpha\delta\hat{h}_1\hat{h}_2\right] = -C(P_w \to P_m) - C(K_w \to P_w), \tag{A2}$$

where $K_w$ and $P_w$ are wave kinetic and potential energy respectively, $C(K_w \to K_m)$, $C(K_w \to P_w)$ and $C(P_w \to P_m)$ are transfer rates given by

$$C(K_w \to K_m) = \int_s \left[\bar{h}_1 \frac{d\bar{u}_1}{dy}\hat{u}_1\hat{v}_1 + \delta\bar{h}_2 \frac{d\bar{u}_2}{dy}\hat{u}_2\hat{v}_2\right] ds, \tag{A3}$$

$$\begin{aligned}C(K_w \to P_w) = \int_s \Bigg[&\bar{h}_1\left(\hat{u}_1 \frac{\partial\hat{p}_1}{\partial x} + \hat{v}_1 \frac{\partial\hat{p}_1}{\partial y}\right) + \delta\bar{h}_2\left(\hat{u}_2 \frac{\partial\hat{p}_2}{\partial x} + \hat{v}_2 \frac{\partial\hat{p}_2}{\partial y}\right) \\ &+ \bar{h}_3\left(\hat{u}_3 \frac{\partial\hat{p}_3}{\partial x} + \hat{v}_3 \frac{\partial\hat{p}_3}{\partial y}\right)\Bigg] ds,\end{aligned} \tag{A4}$$

$$C(P_w \to P_m) = \int_s \left[\bar{u}_1\hat{p}_1 \frac{\partial\hat{h}_1}{\partial x} + \delta\bar{u}_2\hat{p}_2 \frac{\partial\hat{h}_2}{\partial x}\right] ds. \tag{A5}$$

Adding A1 and A2, we obtain the wave energy equation:

$$\frac{\partial}{\partial t}(K_w + P_w) = -C(P_w \to P_m) - C(K_w \to K_m). \tag{A6}$$

As usual, $-C(P_w \to P_m)$ represents the energy conversion rate from mean to perturbation potential energy (the signature of baroclinic instability) and $-C(K_w \to K_m)$ from mean kinetic energy to perturbation kinetic energy (the signature of barotropic instability).

Eq. A5 can be also written as

$$C(P_m \to P_w) = \int_s (\bar{u}_1 - \bar{u}_2)\left[\hat{p}_1 \frac{\partial\hat{p}_2}{\partial x}\right] ds + \int_s \frac{1}{\alpha}\bar{u}_2\left[\hat{p}_2 \frac{\partial\hat{p}_3}{\partial x}\right] ds. \tag{A7}$$

If $\hat{p}_1$, $\hat{p}_2$ and $\hat{p}_3$ are exactly in phase, $C(P_m \to P_w)$ vanishes. Therefore (A7) expresses the baroclinic energy conversion mechanism through the phase lag of the perturbation pressures.

*b. Application to the isolated front.* We calculated energy conversion terms $C(K_m \rightarrow K_w)$, $C(P_m \rightarrow P_w)$ for the isolated front. We found that $C(K_m \rightarrow K_w)$ is about 32.0% of $C(P_m \rightarrow P_w)$ and positive. This shows that the unstable wave draws energy mainly from the mean potential energy, and kinetic energy transfer is from mean flow to perturbation, not vice versa. Of the total transfer $C(K_m \rightarrow K_w)$ plus $C(P_m \rightarrow P_w)$, about 75% is from mean flow potential energy, the rest from mean flow's kinetic energy.

*c. Application to the coastal front.* The energy conversion terms $C(K_m \rightarrow K_w)$, $C(P_m \rightarrow P_w)$ for the coastal front were also calculated. The results were much the same as for the isolated front. When bottom topography is included in the coastal model, the energy conversion terms $C(K_m \rightarrow K_w)$, $C(P_m \rightarrow P_w)$ change. In that case, $C(K_m \rightarrow K_w)$ is only about 19% of $C(P_m \rightarrow P_w)$ and the sign is negative in the three-layer region. In other words, the unstable wave draws energy from mean potential energy and some portion of that energy is transferred back to mean kinetic energy in the three-layer region via "negative viscosity."

## REFERENCES

Bane, J. M., O. B. Brown, R. H. Evans and P. Hamilton. 1988. Gulf Stream remote forcing of Shelfbreak Currents in the Mid-Atlantic Bight. Geophys. Res. Letts., *15,* 405–407.

Barth, J. A. 1987. Stability of a coastal upwelling front over topography. Ph.D. Dissertation, MIT/WHOI-87-48, 187 pp.

Bower, A. S., H. T. Rossby and J. L. Lillibridge. 1985. The Gulf Stream—Barrier or Blender? J. Phys. Oceanogr., *15,* 24–32.

Bower, A. S., R. O'Gara and H. T. Rossby. 1986. RAFOS pilot studies in the Gulf Stream: 1984–1985. Tech. Rep. No. 86-7, Graduate School of Oceanography, University of Rhode Island, 110 pp.

Bower, A. S. and T. Rossby. 1989. Evidence of cross-frontal exchange processes in the Gulf Stream based on isopycnal RAFOS float data. J. Phys. Oceanogr., *19,* 1177–1190.

Chia, F., R. W. Griffiths and P. F. Linden. 1982. Laboratory experiments on fronts. Part II: The formation of cyclonic eddies at upwelling fronts. Geophys. Astrophys. Fluid Dyn., *19,* 189–206.

Csanady, G. T. 1982. On the structure of transient upwelling events. J. Phys. Oceanogr., *12,* 84–96.

Csanady, G. T. and P. Hamilton. 1988. Circulation of slopewater. Cont. Shelf Res., *8,* 565–624.

Cushman-Roisin, B. 1993. Trajectories in Gulf Stream meanders. J. Geophys. Res., *98,* 2543–2544.

Fedorov, K. N. 1986. The Physical Nature and Structure of Oceanic Fronts. Springer-Verlag, New York, 333 pp.

Garvine, R. W. 1984. Propagating long waves on oceanic density fronts: an analytic model. J. Phys. Oceanogr., *14,* 1590–1599.

—— 1988. Flow field properties of long, propagating frontal wave. J. Phys. Oceanogr., *18,* 788–792.

Gerald, C. F. and P. O. Wheatly. 1985. Applied Numerical Analysis. Addison-Wesly, Massachusetts, 340 pp.

Gill, A. E. 1982. Atmosphere-Ocean Dynamics. Academic Press, New York, 662 pp.

Griffiths, R. W. and P. F. Linden. 1982. Laboratory experiments on fronts. Part I: Density-driven boundary currents. Geophys. Astrophys. Fluid Dyn., *19,* 159–187.

Huang, R. X. and H. Stommel. 1990. Cross sections of a two-layer inertial Gulf Stream. J. Phys. Oceanogr., *20,* 907–911.

Iselin, C. O'D. 1936. A study of the circulation of the western North Atlantic. Pap. in Phys. Oceanogr. and Meteor., *4,* 101 pp.

Killworth, P. D. 1983. Long-wave instability of an isolated front. Geophys. Astrophys. Fluid Dyn., *25,* 235–258.

Killworth, P. D., N. Paldor and M. E. Stern. 1984. Wave propagation and growth on a surface front in a two-layer geostrophic current. J. Mar. Res., *42,* 761–785.

Kubokawa, A. 1985. Instability of a geostrophic front and its energetics. Geophys. Astrophys. Fluid Dyn., *33,* 223–257.

Lee, S. K. 1993. Instability waves in the Gulf Stream front and its thermocline layer. M.Sc. Thesis, Old Dominion University, 64 pp.

McLellan, H. J., L. Lauzier and W. B. Bailey. 1953. The slope water off the Scotian Shelf. J. Fish. Res. Bd. Canada, *10,* 155–178.

Oey, L. Y. 1988. A model of Gulf Stream frontal instabilities, meanders and eddies along the continental slope. J. Phys. Oceanogr., *18,* 211–229.

Orlanski, I. 1968. Instability of frontal waves. J. Atmos. Sci., *25,* 178–200.

—— 1969. The influence of bottom topography on the stability of jets in a baroclinic fluid. J. Atmos. Sci., *26,* 1216–1232.

Ou, H. W. 1986. On the energy conversion during geostrophic adjustment. J. Phys. Oceanogr., *16,* 2203–2204.

Paldor, N. 1983. Linear stability and stable modes of geostrophic fronts. Geophys. Astrophys. Fluid Dyn., *24,* 299–326.

Pedlosky, J. 1962. Baroclinic instability in two-layer systems. Tellus, *15,* 20–25.

—— 1987. Geophysical Fluid Dynamics. Springer-Verlag, New York, 710 pp.

Phillips, N. A. 1954. Energy transformations and meridional circulations associated with simple baroclinic waves in a two-level, quasi-geostrophic model. Tellus, *11,* 273–286.

Rossby, C. G. 1936. Dynamics of steady ocean currents in the light of experimental fluid mechanics. Papers in Phys. Oceanogr. and Meteor., *5,* 43 pp.

Stommel, H. 1965. The Gulf Stream: A Physical and Dynamic Description. Univ. California Press, 248 pp.

Van Heijst, G. J. F. 1985. A geostrophic adjustment model of a tidal mixing front. J. Phys. Oceanogr., *15,* 1182–1190.

Watts, D. R. and W. E. Johns. 1982. Gulf Stream meanders: Observations on propagating and growth. J. Geophys. Res., *87,* 9467–9476.

Received: *30 November, 1993;* revised: *24 April, 1994.*